Burak Kılıç [ID] [,1] Özge Özdemir [ID] [1]

Vibration and stability analyses of functionally graded beams

Design considerations, material properties and dynamic properties of engineering applications, rotating components, turbine blades, helicopter blades, etc., have significant effects on system efficiency. Structures made of functionally graded materials have recently begun to take place in such engineering applications, resulting from the development of composite material technology. In this study, vibration and buckling characteristics of axially functionally graded beams whose material properties change along the beam length is analyzed. Beam structural formulations and functionally graded material formulations are obtained for the Classical and the First Order Shear Deformation Theories. Finite element models are derived to carry out the vibratory and stability characteristic analyses. Effects of several parameters, i.e., rotational speed, hub radius, material properties, power law index parameter and boundary conditions are investigated and are displayed in several figures and tables. The calculated results are compared with the ones in open literature and very good agreement is observed.

1. Introduction

Rotating structures are subjected to vibration for various reasons. Determination of the natural frequencies and the mode shapes is required to perform the vibration analysis in the design process of such structures correctly. Many numerical and approximate calculation methods are used in the vibration and natural frequency calculations and the Finite Element Method (FEM) is among the mostly used methods.

Air and space vehicles, wind turbines, helicopter blades, turbine rotors, defense and civil industries, ship and automotive sectors are among the engineering areas

---

✉ Özge Özdemir, e-mail: ozdemirozg@itu.edu.tr

[1]Istanbul Technical University, Faculty of Aeronautics and Astronautics, Istanbul, Turkey. e-mail (B.K.): kilicburak@itu.edu.tr; ORCIDs: B.K: 0000-0003-1290-5387; Ö.Ö.: 0000-0002-4755-2094

where composite materials have been mostly preferred due to their advantages, i.e., light weight and high strength/stiffness-to-weight ratios. However, composite materials have some limitations. For instance, stress concentration near interlayer surfaces is high because of the sudden changes in mechanical properties, and this limitation may cause severe material failures. Moreover, the adhesive layer may get cracked when the temperature is low and it may creep at high temperature. Functionally graded materials, FGMs, are considered to be the new generation composite materials. The variational character of their material properties is continuous through the structure, so stress concentrations do not occur. Survivability in high temperatures by maintaining structural integrity is among the outstanding properties of FGMs. Although many different material combinations have been studied for FGMs, the most widely used one is the ceramic-metal combination where the ceramic reduces heat transfer to protect metal from corrosion and oxidation, whereas metal provides strength, higher fracture toughness, etc.

Structural components used in engineering are mostly beams and beam-like structures. Different material types, i.e., homogeneous, composite, functionally graded, etc., are used in these structural components to meet different engineering design requirements. Both in conventional structural applications and in advanced structural applications, including electric-thermal-structural systems, FGMs are commonly used as harvesters, sensors and actuators. Therefore, many researchers have been studying these materials for different application areas. Due to the increasing application trend of FGMs, different beam theories have been used to examine the vibration properties of Functionally Graded Beams (FGBs). The Euler-Bernoulli theory is the simplest theory that can be applied to slender FGBs. The Timoshenko theory is used for the case of either short beams or high frequency applications where the transverse shear deformation effect is considered.

The concept of FGMs was originated from a team of material scientists working on thermal barrier materials [1] and nowadays, production areas and application fields are increasing day by day with the development of additive manufacturing technology and powder metallurgy of the material properties. In [2], authors studied FGM beams with simply-simply supported end conditions under the effect of transverse loading where the beam elasticity modulus changes through the beam thickness. Free vibration analysis of FGM beams with simply supported end conditions and with modulus of elasticity changing with respect to a power and an exponential rule in the transverse direction is investigated analytically in [3]. A new beam element has been developed by [4] to study the thermoelastic behavior of functionally graded beam structures. In [5], authors optimized the natural frequencies of FGM beams by changing the material distribution via a genetic algorithm methodology. Free and forced vibration of a nonuniform FGM beam that is thermally prestressed is analyzed in [6]. In [7], authors employed a formulation accounting for shear-deformability and nonlinear strain–displacements relationships to study the dynamic behavior of rotating FGM beams. Both the free vibration and the harmonically forced vibration of FGM Euler-Bernoulli beams

are studied in [8]. Out-of-plane free vibration of curved beams made of FGM is analyzed in [9] where temperature dependent material properties are considered. In [10], authors studied free vibration of nonuniform axially functionally graded beams with variable flexural rigidity and mass density. Free vibration and stability analyses of Timoshenko beams with nonuniform cross-sections were studied in [11] by employing an energy-based finite element solution. In [12], authors examined functionally graded column which have fixed-free end conditions and which is subjected to a compressive axial load. Free vibration and stability of axially functionally graded Euler-Bernoulli beams that taper in different planes are studied in [13]. Generalized isoparametric graded finite element formulation is studied in Ref. [14] for plates where graded elements are used. By using isoparametric shape functions, the material properties can be interpolated from the nodal material properties of the element. Additionally, several review papers have been published in recent years about the modeling procedures, stability and vibration characteristics of FGM structures [15, 16].

In this study, FG beams whose material distribution changes in the spanwise direction are modeled. Free vibration and buckling analyses are performed. Beam models with different boundary conditions and different material distribution properties are investigated. For developing the mathematical models and for analyzing different cases, Finite Element Method (FEM) is used. The beam formulations are derived for both Euler-Bernoulli and Timoshenko beam theories to inspect the effect of different parameters on the vibration characteristics. For each beam theory, both stiffness and mass matrices are derived from the energy expressions. In the solution part, effects of different parameters such as hub rotating speed, hub radius, material distribution properties, power law index parameter and boundary conditions are investigated.

2. Functionally graded beam model

In this study, vibration and buckling analyses are carried out for rotating/non-rotating beams which contain two different material properties in different compositions and whose material properties change along the beam axis, as shown in Fig. 1.

Here, a beam of length L, of cross-sectional dimensions b and h, rotating with a constant speed Ω in rad/sec, is fixed to a rigid hub of radius R at point O. The origin of the right-handed Cartesian coordinate system is located at the root of the beam and the y-axis is directed along the beam while the rotational axis and the z-axis are parallel.

The beam is modeled with constant cross-sectional dimensions and variable material properties along the x-axis. The beam model has two different material properties, i.e., ceramic and metal, in different compositions from the fixed to the free end.
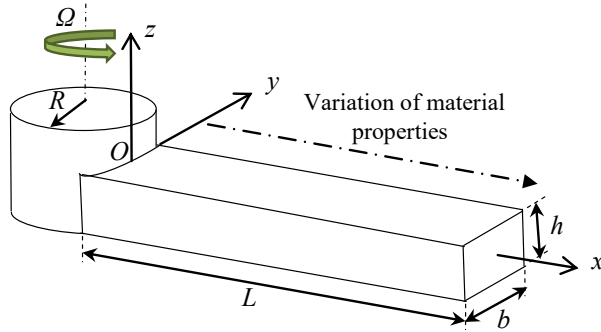
Fig. 1. Rotating axially functionally graded beam model

Beam material properties vary continuously along the x-axis, via a simple power law given by Eq. (1)

$$T(x) = (T_R - T_L)\left(\frac{x}{L}\right)^n + T_L, \quad n \geqslant 0 \tag{1}$$

Here $T(x)$ is the effective material property such as the modulus of elasticity E, shear modulus G and material density ρ. Moreover, n is a non-negative power law index parameter that dictates the material variation profile along the beam axis.

$$E(x) = (E_R - E_L)\left(\frac{x}{L}\right)^n + E_L, \tag{2a}$$

$$G(x) = (G_R - G_L)\left(\frac{x}{L}\right)^n + G_L, \tag{2b}$$

$$\rho(x) = (\rho_R - \rho_L)\left(\frac{x}{L}\right)^n + \rho_L. \tag{2c}$$

Here $(\ )_R$ and $(\ )_L$ are the material properties at the right hand side and left hand side of the beam, respectively, as shown in Fig. 2.
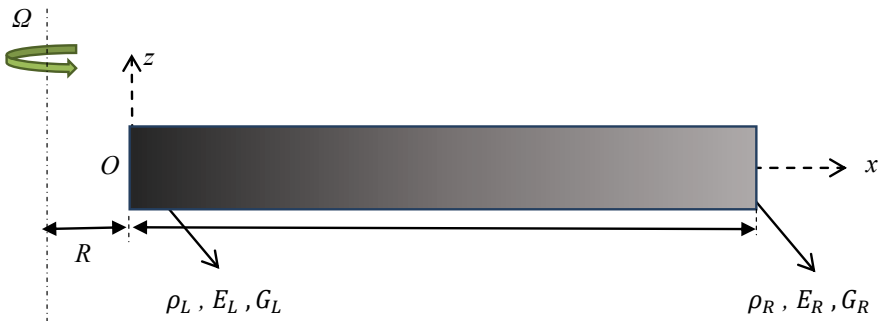

Fig. 2. Material variation in an axially functionally graded beam model

The gradation functions represented by Eqs. (2a)–(2c) are the expressions to be used to build up the mathematical model of a functionally graded beam and to study the mechanical properties as a preliminary approach. They are mathematically correct and can be used to build up the mathematical models but they do not reflect real morphological microstructure of FGM.

3. Energy expressions

In this section, energy expressions are given both for a rotating Euler-Bernoulli beam and a rotating Timoshenko beam. Details of the derivations can be found in the studies of [17] and [18].

The potential energy expressions of axially functionally graded beam models that rotate with a constant angular speed Ω are given in Eq. (3a) for the Euler-Bernoulli beam U_E and in Eq. (3b) for the Timoshenko beam U_T.

$$U_E = \frac{1}{2} \int_0^L \left[E(x)I_y(\theta')^2 + F_{CF}(x)(w')^2 \right] \mathrm{d}x + C_1, \tag{3a}$$

$$U_T = \frac{1}{2} \int_0^L \left[E(x)I_y(\theta')^2 + kAG(x)\left(w' - \theta\right)^2 + F_{CF}(x)(w')^2 \right] \mathrm{d}x + C_2, \tag{3b}$$

where F_{CF} is the centrifugal force, k is the shear correction factor which is 5/6 for rectangular cross-sections, I_y is the moment of inertia about the y-axis, A is the beam cross-sectional area, w is the flapwise bending deflection and θ is the rotation due to flapwise bending. C_1 and C_2 are the integration constants.

Here the centrifugal force is

$$F_{CF}(x) = \int_x^L \rho(x)A\Omega^2(R + x)\,\mathrm{d}x. \tag{4}$$

The kinetic energy expressions of axially functionally graded beam models that rotate with a constant angular speed are given in Eq. (5a) for the Euler-Bernoulli beam T_E and in Eq. (5b) for the Timoshenko beam T_T

$$T_E = \frac{1}{2} \int_0^L \left(\rho A\dot{w}^2 + \rho I_y\left(\dot{w}'\right)^2 + \rho I_y\Omega^2(w')^2 \right)\mathrm{d}x + D_1, \tag{5a}$$

$$T_T = \frac{1}{2} \int_0^L \left(\rho A\dot{w}^2 + \rho I_y\dot{\theta}^2 + \rho I_y\Omega^2\theta^2 \right)\mathrm{d}x + D_2. \tag{5b}$$

Here D_1 and D_2 are the integration constants.

4. Finite element modeling

Finite element formulation of a rotating axially functionally graded beam, i.e., Fig. 3, that undergoes flapwise bending deflection is carried out in this section.
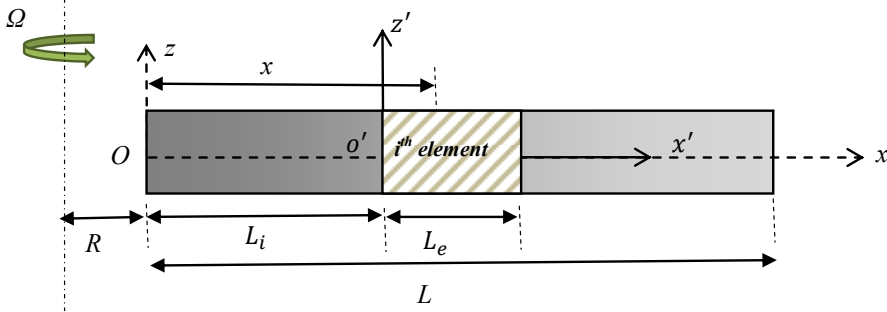

Fig. 3. Finite element model of a rotating axially functionally graded beam

Here L_i is the offset of each element from the rotational axis, L_e is the element length, xyz is the global coordinate system while $x'y'z'$ is the local coordinate system. The element length can vary along the beam length depending on the analyzed case, but in this study the beam is divided into elements of equal length.

In the case of a rotating beam, additional terms appear in the element matrices due to the centrifugal force. Considering Fig. 3, the centrifugal force given by Eq. (4) can be expressed in finite element form as follows

$$F_{CF}(x) = \rho A \Omega^2 \left[R \left(L - L_i - x' \right) + \frac{1}{2} \left(L - L_i - x' \right) \left(L - L_i + x' \right) \right], \qquad \text{(6a)}$$

$$L_i = (i - 1) \frac{L}{N_e} . \qquad \text{(6b)}$$

Here, L is the length of the beam and N_e is the number of elements used in the finite element formulation.

4.1. Finite element modeling of the Euler-Bernoulli beam

The finite element model of an Euler-Bernoulli beam element is given in Fig. 4.

A two-nodded beam element that has four degrees of freedom is considered where w is the flapwise bending displacement and θ is the rotational angle due to flapwise bending displacement.

Polynomials of appropriate order are defined for the displacement field as follows

$$w = a_0 + a_1 x + a_2 x^2 + a_3 x^3, \qquad \text{(7a)}$$

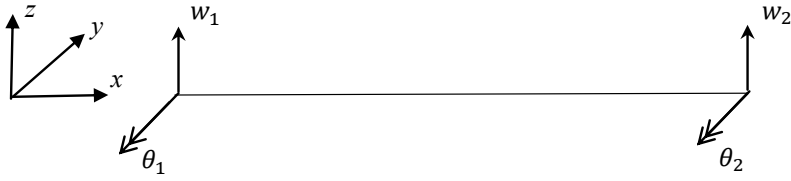$$\theta = w' = a_1 + 2a_2 x + 3a_3 x^2 . \qquad \text{(7b)}$$

Fig. 4. Finite element model of the Euler-Bernoulli beam element

Considering the displacement field polynomials given by Eq. (7a) and Eq. (7b), the nodal displacements are determined as the displacement values at the 1st node of the element $x = 0$ and at the 2nd node $x = L$, respectively. These are given in matrix form as follows

$$\begin{Bmatrix} w_1 \\ \theta_1 \\ w_2 \\ \theta_2 \end{Bmatrix} = \begin{bmatrix} 1 & 0 & 0 & 0 \\ 0 & 1 & 0 & 0 \\ 1 & L_e & L_e^2 & L_e^3 \\ 0 & 1 & 2L_e & 3L_e^2 \end{bmatrix} \begin{Bmatrix} a_0 \\ a_1 \\ a_2 \\ a_3 \end{Bmatrix}. \tag{8}$$

Here, $(\ )_1$ are the displacement values of the 1st node while $(\ )_2$ are the displacements on the 2nd node.

The relation between the displacement field and the nodal displacements is

$$\{q\} = [N]\{q_e\}, \tag{9}$$

where for the present beam model, expressions of the displacements $\{q\}$, the nodal displacements $\{q_e\}$ and the matrix of the shape functions $[N]$ are given by

$$\{q\} = \{w \quad \theta\}^T, \tag{10a}$$

$$\{q_e\} = \{w_1 \quad \theta_1 \quad w_2 \quad \theta_2\}^T, \tag{10b}$$

$$[N] = \begin{bmatrix} N_w & N_\theta \end{bmatrix}^T, \tag{10c}$$

where the expressions of the shape functions are

$$[N_w] = \left\{ 1 - \frac{3x^2}{L_e^2} - \frac{2x^3}{L_e^3} \quad x - \frac{2x^2}{L_e} + \frac{x^3}{L_e^2} \quad \frac{3x^2}{L_e^2} - \frac{2x^3}{L_e^3} \quad -\frac{x^2}{L_e} + \frac{x^3}{L_e^2} \right\}, \tag{11a}$$

$$[N_\theta] = \left\{ \frac{6x}{L_e^2} + \frac{6x^2}{L_e^3} \quad 1 - \frac{4x}{L_e} + \frac{3x^2}{L_e^2} \quad \frac{6x}{L_e^2} - \frac{6x^2}{L_e^3} \quad -\frac{2x}{L_e} + \frac{3x^2}{L_e^2} \right\}. \tag{11b}$$

Here, $[N_w]$ and $[N_\theta]$ are the shape functions associated with the flapwise bending w and the angle due to flapwise bending θ, respectively. The transpose of a matrix is given by $[\ ]^T$.

Considering the effect of centrifugal force and substituting the shape functions, i.e., Eq. (11a) and Eq. (11b), into the potential and kinetic energy expressions, i.e.,

Eq. (3a) and Eq. (5a), the element stiffness matrix $[\mathbf{K^e}]$ and element mass matrix $[\mathbf{M^e}]$ are obtained for the Euler-Bernoulli beam model as follows

$$[\mathbf{K^e}] = \frac{1}{2} \int_0^{L_e} \left(E(x)I_y \left[\frac{dN_\theta}{dx}\right]^T \left[\frac{dN_\theta}{dx}\right] + F_{CF}(x) \left[\frac{dN_w}{dx}\right]^T \left[\frac{dN_w}{dx}\right] \right) dx, \quad (12a)$$

$$[\mathbf{M^e}] = \frac{1}{2} \int_0^{L_e} \left(\rho(x)A\,[N_w]^T\,[N_w] + \rho(x)I_y\,[N_\theta]^T\,[N_\theta] \right) dx. \quad (12b)$$

Here, the element stiffness matrix is derived from the potential energy expression, i.e., Eq. (3a) and the element mass matrix is derived from the kinetic energy expression, i.e., Eq. (5a).

Considering Eq. (12a), components of the element stiffness matrix can be classified as the flextural stiffness matrix $[\mathbf{K^e}]_\mathbf{f}$ and the geometric stiffness matrix $[\mathbf{K^e}]_\mathbf{g}$ whose expressions are as follows

$$[\mathbf{K^e}]_\mathbf{f} = \frac{1}{2} \int_0^L \left(E(x)I_y \left[\frac{dN_\theta}{dx}\right]^T \left[\frac{dN_\theta}{dx}\right] \right) dx, \quad (13a)$$

$$[\mathbf{K^e}]_\mathbf{g} = \frac{1}{2} \int_0^L F_{CF}(x) \left[\frac{dN_w}{dx}\right]^T \left[\frac{dN_w}{dx}\right] dx. \quad (13b)$$

In the case of rotating beams, the centrifugal force $F_{CF}(x)$ is modeled as a tensile axially distributed load along the structure. However, in the case of buckling, the centrifugal force is modeled as a compressive axially distributed load.

4.2. Finite element modeling of the Timoshenko beam

The finite element model of a rotating Timoshenko beam element is given in Fig. 5. Here, a two-nodded beam element that has six degrees of freedom is considered, where w is the flapwise bending displacement, θ is the rotation angle due to flapwise bending and φ is shear angle which is the result of Timoshenko beam formulation.

Fig. 5. Finite element model of the Timoshenko beam element

Polynomials of appropriate order are defined for the displacement field as follows

$$w = a_0 + a_1 x + a_2 x^2 + a_3 x^3, \tag{14a}$$

$$\varphi = a_4 + a_5 x, \tag{14b}$$

$$\theta = w' - \varphi = a_1 - a_4 + (2a_2 - a_5)\, x + 3a_3 x^2. \tag{14c}$$

Considering the displacement field polynomials given by Eqs. (14a)–(14c), the nodal displacements are determined as the displacement values at the 1st node of the element $x = 0$ and at the 2nd node $x = L$, respectively. These are given in a matrix form as follows

$$\begin{Bmatrix} w_1 \\ \theta_1 \\ \varphi_1 \\ w_2 \\ \theta_2 \\ \varphi_2 \end{Bmatrix} = \begin{bmatrix} 1 & 0 & 0 & 0 & 0 & 0 \\ 0 & 1 & 0 & 0 & -1 & 0 \\ 0 & 0 & 0 & 0 & 1 & 0 \\ 1 & L_e & L_e^2 & L_e^3 & 0 & 0 \\ 0 & 1 & 2L_e & 3L_e^2 & -1 & -L_e \\ 0 & 0 & 0 & 0 & 1 & L_e \end{bmatrix} \begin{Bmatrix} a_0 \\ a_1 \\ a_2 \\ a_3 \\ a_4 \\ a_5 \end{Bmatrix}, \tag{15}$$

where for the present beam model, expressions of the displacements $\{q\}$, the nodal displacements $\{q_e\}$

$$\{q\} = \{w \quad \theta \quad \varphi\}^T, \tag{16a}$$

$$\{q_e\} = \{w_1 \quad \theta_1 \quad \varphi_1 \quad w_2 \quad \theta_2 \quad \varphi_2\}^T, \tag{16b}$$

$$[N] = \begin{bmatrix} N_w & N_\theta & N_\varphi \end{bmatrix}^T, \tag{16c}$$

where the matrix of the shape functions $[N]$ are given by

$$[N_w] = \left\{ 1 - \frac{3x^2}{L_e^2} + \frac{2x^3}{L_e^3} \quad x - \frac{2x^2}{L_e} + \frac{x^3}{L_e^2} \quad x - \frac{2x^2}{L_e} + \frac{x^3}{L_e^2} \right.$$
$$\left. \frac{3x^2}{L_e^2} - \frac{2x^3}{L_e^3} \quad -\frac{x^2}{L_e} + \frac{x^3}{L_e^2} \quad -\frac{x^2}{L_e} + \frac{x^3}{L_e^2} \right\}, \tag{17a}$$

$$[N_\theta] = \left\{ -\frac{6x}{L_e^2} + \frac{6x^2}{L_e^3} \quad 1 - \frac{4x}{L_e} + \frac{3x^2}{L_e^2} \quad -\frac{3x}{L_e} + \frac{3x^2}{L_e^2} \right.$$
$$\left. \frac{6x}{L_e^2} - \frac{6x^2}{L_e^3} \quad -\frac{2x}{L_e} + \frac{3x^2}{L_e^2} \quad -\frac{3x}{L_e} + \frac{3x^2}{L_e^2} \right\}, \tag{17b}$$

$$[N_\varphi] = \left\{ 0 \quad 0 \quad 1 - \frac{x}{L_e} \quad 0 \quad 0 \quad \frac{x}{L_e} \right\}. \tag{17c}$$

Here $[N_w]$, $[N_\theta]$ and $[N_\varphi]$ are the shape functions associated with the flapwise bending w, angle due to flapwise bending θ and shear angle φ, respectively.

4.3. Stiffness and mass matrices

Considering the effect of centrifugal force and substituting the shape functions, i.e., Eq. (17a)–(17c) into the potential and kinetic energy expressions, i.e., Eq. (3b) and Eq. (5b), the element stiffness matrix $[\mathbf{K^e}]$ and element mass matrix $[\mathbf{M^e}]$ are obtained for the Timoshenko beam model as follows

$$[\mathbf{K^e}] = \frac{1}{2} \int_0^L \left(E(x)I_y \left[\frac{\mathrm{d}N_\theta}{\mathrm{d}x}\right]^T \left[\frac{\mathrm{d}N_\theta}{\mathrm{d}x}\right] + kAG(x) \left(\left[\frac{\mathrm{d}N_w}{\mathrm{d}x}\right] - N_\theta\right)^T \right.$$

$$\left. \cdot \left(\left[\frac{\mathrm{d}N_w}{\mathrm{d}x}\right] - N_\theta\right) + F_{CF}(x) \left[\frac{\mathrm{d}N_w}{\mathrm{d}x}\right]^T \left[\frac{\mathrm{d}N_w}{\mathrm{d}x}\right] \right) \mathrm{d}x, \tag{18a}$$

$$[\mathbf{M^e}] = \frac{1}{2} \int_0^L \left(\rho(x)A \left[N_w\right]^T \left[N_w\right] + \rho(x)I_y \left[N_\theta\right]^T \left[N_\theta\right] \right) \mathrm{d}x. \tag{18b}$$

Here, the element stiffness matrix is derived from the potential energy expression, i.e., Eq. (3b) and the element mass matrix is derived from the kinetic energy expression, i.e., Eq. (5b).

Comparing Eq. (12a) and Eq. (18a), it is noticed that for the Timoshenko beam model the element stiffness matrix has one more component, i.e., shear stiffness matrix, i.e., Eq. (19), due to the shear effects.

$$[\mathbf{K^e}]_{\mathbf{s}} = \frac{1}{2} \int_0^L kAG(x) \left(\left[\frac{\mathrm{d}N_w}{\mathrm{d}x}\right] - N_\theta\right)^T \left(\left[\frac{\mathrm{d}N_w}{\mathrm{d}x}\right] - N_\theta\right) \mathrm{d}x. \tag{19}$$

5. Free vibration and buckling analyses

Depending on the number of elements used in the finite element modeling, all the element matrices are assembled by considering the finite element rules to obtain the global matrices. The boundary conditions are applied to the global matrices to get the reduced matrices and the following matrix system of equations is obtained

$$[\mathbf{M}]\{\ddot{q}\} + [\mathbf{K}]\{q\} = \{0\}, \tag{20}$$

where $[\mathbf{M}]$ and $[\mathbf{K}]$ are the reduced global mass and stiffness matrices, respectively. The stiffness matrix is a combination of the flexural, shear and geometric stiffness matrices, as follows

$$[\mathbf{K}] = [\mathbf{K}]_{\mathbf{f}} + [\mathbf{K}]_{\mathbf{s}} + [\mathbf{K}]_{\mathbf{g}}, \tag{21}$$

where $[\mathbf{K}]_{\mathbf{f}}$ is the global flexural stiffness matrix, $[\mathbf{K}]_{\mathbf{s}}$ is the global shear stiffness matrix and $[\mathbf{K}]_{\mathbf{g}}$ is the global geometric stiffness matrix.

Free vibration analysis is applied to Eq. (20) to calculate the natural frequencies by solving the following eigenvalue problem, i.e., Eq. (22) where Φ is the mode shape. Natural frequencies are calculated for the Euler–Bernoulli and Timoshenko beam models having different boundary conditions.

$$\left([\mathbf{K}]_\mathbf{f} + [\mathbf{K}]_\mathbf{s} + [\mathbf{K}]_\mathbf{g} - \omega^2 [\mathbf{M}]\right) \Phi = 0. \tag{22}$$

Buckling analysis is carried out by solving a different eigenvalue problem, i.e., Eq. (24). The critical buckling load and the corresponding natural frequency can be calculated for the Euler–Bernoulli and Timoshenko beam models having different boundary conditions

$$\left([\mathbf{K}]_\mathbf{f} + [\mathbf{K}]_\mathbf{s} - \lambda [\mathbf{K}]_\mathbf{g}\right) \Phi = 0, \tag{23}$$

where λ is the eigenvalue and $P_{cr} = -\lambda P$ is the critical buckling load and P is the axial load, i.e., the negative centrifugal force $F_{CF}(x)$ as defined in this study.

6. Results and discussions

In this section, flapwise bending vibration and buckling analyses of both Euler–Bernoulli and Timoshenko beams that have material variation in the axial direction are carried out. Several parameters, i.e., power law index parameter for material distribution, dimensionless angular speed, dimensionless hub radius and different boundary conditions are considered. The calculated results are given in several tables and figures.

The dimensionless parameters used in the tables and graphics are

$$\overline{\omega} = \omega\sqrt{\frac{\rho_0 A_0 L^4}{E_0 I_{y0}}}, \tag{24a}$$

$$\overline{\Omega} = \Omega\sqrt{\frac{\rho_0 A_0 L^4}{E_0 I_{y0}}}, \tag{24b}$$

$$\overline{P}_{cr} = P_{cr}\frac{L^2}{E_0 I_{y0}}, \tag{24c}$$

$$r = \sqrt{\frac{I_{y0}}{A_0 L^2}}, \tag{24d}$$

$$\sigma = \frac{R}{L}, \tag{24e}$$

where the properties given in the parenthesis $(\ldots)_0$ are the ones defined at the root of the beam where $x = 0$. Here, $\overline{\omega}$ is the dimensionless natural frequency, $\overline{\Omega}$ is the dimensionless angular speed, $\overline{P}_{cr}$ is the dimensionless critical buckling load, r is the inverse of the slenderness ratio and σ is the dimensionless hub radius.

6.1. Results for homogeneous material distribution

In this section, vibration and buckling characteristics are examined for both homogeneous Euler-Bernoulli and Timoshenko beams and the results are tabulated for different cases. The beam model used for the analysis is shown in Fig. 6.
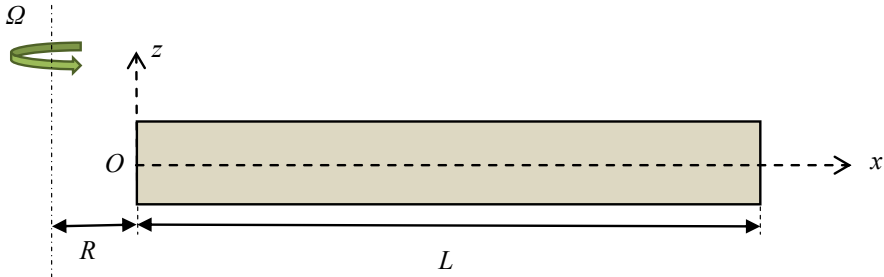

Fig. 6. Homogeneous beam model

Case 1: Dimensionless natural frequencies of a rotating homogeneous Euler–Bernoulli beam with fixed-free end conditions are calculated. The beam properties are given in Table 1. In Table 2, the calculated results are validated with the exact results of Ref. [20] for the stationary case ($\overline{\Omega} = 0$) and the rotating cases ($\overline{\Omega} = 3, 6$ and 12).

When Table 2 is examined, it is noticed that, as the dimensionless angular speed $\overline{\Omega}$ increases, the natural frequencies increase. This is because of the stiffening

Table 1.

Geometrical and material properties of rotating homogeneous Euler–Bernoulli beam [19]

Elasticity modulus E	70 GPa	Beam length L	3 m
Material density ρ	3200 kg/m^3	Beam height h	0.0789 m
Poisson's ratio ν		0.3	

Table 2.

Dimensionless natural frequencies for rotating homogeneous Euler–Bernoulli beam (Fixed-Free)

Dimensionless angular speed	Mode	Natural frequencies, $\overline{\omega}$		Mode	Natural frequencies, $\overline{\omega}$	
		Ref. [20]	Present		Ref. [20]	Present
$\overline{\Omega} = 0$	1st	3.5160	3.51554	2nd	22.0345	22.0139
	3rd	61.6972	61.5602	4th	120.902	120.407
$\overline{\Omega} = 3$	1st	4.7973	4.79666	2nd	23.3203	23.2984
	3rd	62.9850	62.8448	4th	122.236	121.735
$\overline{\Omega} = 6$	1st	7.3604	7.35949	2nd	26.8091	26.7835
	3rd	66.6840	66.5344	4th	126.140	125.623
$\overline{\Omega} = 12$	1st	13.1702	13.1688	2nd	37.6031	37.566
	3rd	79.6145	79.431	4th	140.534	139.952

effect of the centrifugal force, i.e., Eq. (4) which is proportional to the square of the dimensional angular speed Ω.

Case 2: Natural frequencies and critical buckling load of a nonrotating homogeneous Euler–Bernoulli beam with fixed-free and hinged-hinged end conditions are calculated. The beam properties are given in Table 3 and the calculated results are tabulated in Table 4 where effects of different boundary conditions are observed.

Table 3.

Geometrical and material properties of homogeneous Euler–Bernoulli beam [13]

Elasticity modulus E	200 GPa	Slenderness ratio r	0.01
Material density ρ	5700 kg/m^3	Beam length L	2.2 m
Poisson's ratio v	0.3	Beam width b	0.1 m

Table 4.

Dimensionless natural frequencies and buckling load for nonrotating homogeneous Euler-Bernoulli beam

Boundary conditions	Mode	Natural frequencies, $\overline{\omega}$	Buckling load, P_{cr}
Fixed-Free	1st	3.515, 3.516*	2.467, 2.467*
	2nd	21.999	
	3rd	61.460	
	4th	120.047	
Hinged-Hinged	1st	9.865, 9.870*	9.870, 9.870*
	2nd	39.401	
	3rd	88.435	
	4th	156.682	

* Ref. [13]

When Table 4 is examined, it is noticed that the beam model with hinged-hinged boundary conditions has higher natural frequencies and buckling load values when compared to the one with fixed-free boundary conditions.

Case 3: Natural frequencies and critical buckling load of a homogeneous nonrotating Timoshenko beam having different boundary conditions is examined. The beam properties are given in Table 5 and the calculated results are tabulated in Table 6.

Table 5.

Geometrical and material properties of homogeneous Timoshenko beam [11]

Elasticity modulus E	200 GPa	Slenderness ratio r	0.01
Material density ρ	5700 kg/m^3	Beam length L	2.2 m
Poisson's ratio v	0.3	Shear correction factor k	5/6

Dimensionless natural frequencies for the Timoshenko beam (Fixed-Free)

Number of elements	Mode	Natural frequencies, $\overline{\omega}$		Mode	Natural frequencies, $\overline{\omega}$	
		Ref. [11]	Present		Ref. [11]	Present
20	1st	3.2272	3.2318	2nd	14.4778	14.6203
	3rd	31.5924	31.9743	4th	48.1968	48.6357
25	1st	3.2272	3.2309	2nd	14.4746	14.5899
	3rd	31.5601	31.8791	4th	48.0935	48.4861
30	1st	3.2272	3.2302	2nd	14.4729	14.5697
	3rd	31.5425	31.816	4th	48.0372	48.388

In Table 6, the calculated results are compared with open literature. The number of elements used in the finite element coding is changed from 20 to 30 to see the convergence of the natural frequencies.

6.2. Results for axially functionally graded material distribution

In this section, vibration characteristics are examined for both Euler–Bernoulli and Timoshenko beams that have axially functionally graded material properties. The beam model used for the analysis is shown in Fig. 7 where the beam material is pure ZrO_2 at the fixed end and it is pure Al at the free end.
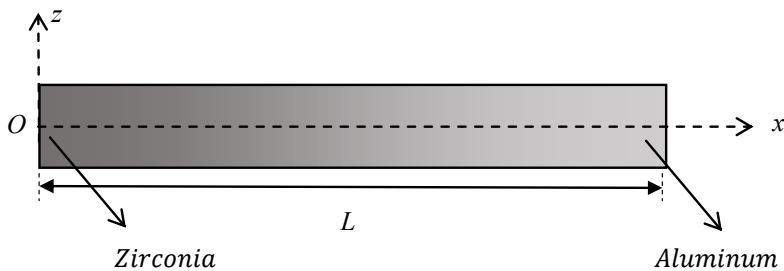

Fig. 7. Axially functionally graded beam model

The material properties of Aluminum and Zirconia that are used for the AFG Euler–Bernoulli beam model are given in Table 7. The beam length is $L = 5$ m, the inverse of the slenderness ratio is $r = 0.01$.

Material properties of the AFG Euler–Bernoulli beam

Property	Zirconia (ZrO_2)	Aluminum (Al)
Elasticity modulus E	200 GPa	70 GPa
Material density ρ	5700 kg/m^3	2702 kg/m^3
Poisson's ratio v	0.3	0.3

Variation of the modulus of elasticity E along the beam length, i.e., Eq. (2b), with respect to the power law index parameter n is shown in Fig. 8. Here it is noticed that the percentage of Zirconia gets higher with the increasing value of the power law index parameter n.
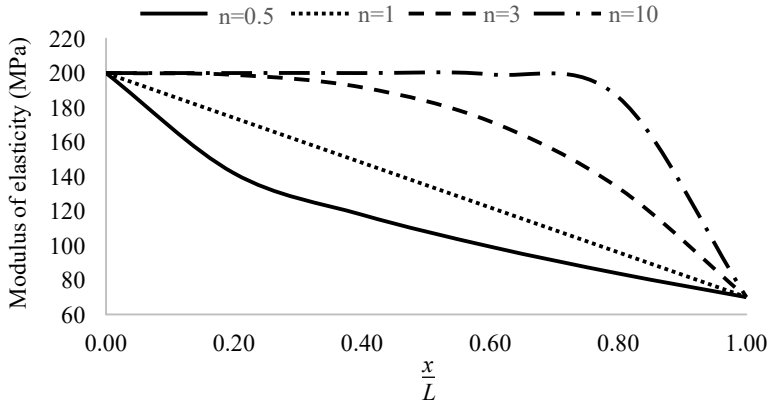

Fig. 8. Variation of the modulus of elasticity with the power law exponent

Case 4: Vibration and buckling analyses of a functionally graded Euler–Bernoulli beam is examined for different boundary conditions. Effects of the power law index parameter n and the boundary conditions on the natural frequencies and the critical buckling load are tabulated in Table 8 and Table 9.

Table 8.

Dimensionless natural frequencies of AFG Euler–Bernoulli beam

Power law index parameter n	Mode	Natural frequencies, $\overline{\omega}$			
		Fixed-Free		Fixed-Fixed	
		Ref. [19]	Present	Ref. [19]	Present
1	1st	6.9717	7.4656	22.7497	23.1725
	2nd	25.6522	26.1552	60.6397	61.0181
	3rd	63.3094	63.644	116.956	116.946
	4th	119.5321	119.337	191.8536	191.044
2	1st	6.9289	7.5487	22.3542	22.7186
	2nd	26.0438	26.6992	60.6611	61.0345
	3rd	64.6733	65.1456	117.9543	117.979
	4th	122.1691	122.073	194.2642	193.54

Case 5: Vibration and buckling characteristics of a functionally graded Timoshenko beam are examined for different boundary conditions.

Table 9.

Dimensionless natural frequencies and critical buckling load of AFG Euler–Bernoulli beam

BC's	Mode	Fixed-Free		Mode	Hinged-Hinged	
n		Natural frequencies, $\overline{\omega}$	Buckling load (P_{cr})		Natural frequencies, $\overline{\omega}$	Buckling load (P_{cr})
0.2	1st	3.698	1.237	1st	8.816	4.291
	2nd	20.968		2nd	35.353	
	3rd	56.794		3rd	79.392	
	4th	109.816		4th	140.686	
0.5	1st	4.091	1.568	1st	9.078	5.203
	2nd	21.977		2nd	36.460	
	3rd	58.591		3rd	81.805	
	4th	112.867		4th	144.897	
0.8	1st	4.260	1.791	1st	9.239	5.915
	2nd	22.477		2nd	37.097	
	3rd	59.593		3rd	83.177	
	4th	114.658		4th	147.279	
1.1	1st	4.326	1.947	1st	9.353	6.493
	2nd	22.768		2nd	37.511	
	3rd	60.264		3rd	84.076	
	4th	115.887		4th	148.845	
1.4	1st	4.340	2.060	1st	9.438	6.970
	2nd	22.961		2nd	37.798	
	3rd	60.778		3rd	84.711	
	4th	116.835		4th	149.959	
1.7	1st	4.329	2.143	1st	9.504	7.367
	2nd	23.103		2nd	38.006	
	3rd	61.202		3rd	85.183	
	4th	117.615		4th	150.794	
2.0	1st	4.301	2.209	1st	9.562, 9.5994*	7.722, 7.8308*
	2nd	23.204		2nd	38.180	
	3rd	61.573		3rd	85.585	
	4th	118.315		4th	151.511	

* Ref. [13]

Effects of the power law index parameter, n and the boundary conditions on the natural frequencies and the critical buckling load are tabulated in Table 10, Table 11 and Table 12. The shear correction factor is $k = 5/6$ for the Timoshenko beam model.

Table 10.

Dimensionless natural frequencies of AFG Timoshenko beam (Fixed-Free)

n	Mode	Natural frequencies, $\overline{\omega}$		n	Mode	Natural frequencies, $\overline{\omega}$	
		Ref. [11]	Present			Ref. [11]	Present
0.3	1st	3.50	3.5222	1.8	1st	3.93	3.9576
	2nd	14.25	14.3333		2nd	15.20	15.4732
	3rd	29.70	30.0593		3rd	31.60	32.0377
	4th	44.50	45.0699		4th	48.00	48.203
0.6	1st	3.79	3.7580	2.1	1st	3.92	3.9458
	2nd	14.75	14.8256		2nd	15.25	15.5248
	3rd	30.40	30.7528		3rd	31.70	32.2145
	4th	45.80	46.0706		4th	48.20	48.5221
0.9	1st	3.90	3.8815	2.4	1st	3.90	3.9283
	2nd	15.00	15.1141		2nd	15.30	15.562
	3rd	30.90	31.2279		3rd	31.80	32.367
	4th	46.00	46.8072		4th	48.30	48.7959
1.2	1st	3.95	3.9388	1.2	1st	3.85	3.9083
	2nd	15.10	15.2884		2nd	15.30	15.5894
	3rd	31.20	31.5676		3rd	32.00	32.5002
	4th	47.00	47.3725		4th	48.40	49.0328
1.5	1st	3.94	3.9585	3.0	1st	3.80	3.9068
	2nd	15.15	15.3991		2nd	15.30	15.2337
	3rd	31.58	31.8274		3rd	32.20	31.5458
	4th	47.70	47.8264		4th	48.50	47.3647

Table 11.

Dimensionless natural frequencies of AFG Timoshenko beam (Fixed-Fixed)

n	Mode	Natural frequencies, $\overline{\omega}$		n	Mode	Natural frequencies, $\overline{\omega}$	
		Ref. [11]	Present			Ref. [11]	Present
0.3	1st	12.87	13.0648	1.8	1st	12.62	12.9043
	2nd	26.78	27.0523		2nd	26.64	27.4202
	3rd	43.30	43.2826		3rd	43.60	44.7496
	4th	59.00	57.8758		4th	59.72	60.4913
0.6	1st	12.79	13.1393	2.1	1st	12.60	12.8521
	2nd	26.74	27.3592		2nd	26.63	27.3899
	3rd	43.4	43.9353		3rd	43.62	44.8206
	4th	59.3	58.9581		4th	59.74	60.6404
0.9	1st	12.73	13.1071	2.4	1st	12.595	12.8107
	2nd	26.7	27.4601		2nd	26.62	27.3639
	3rd	43.49	44.2982		3rd	43.64	44.8741
	4th	59.5	59.5987		4th	59.78	60.7522
1.2	1st	12.68	13.0393	2.7	1st	12.592	12.779
	2nd	26.67	27.4724		2nd	26.61	27.3432
	3rd	43.55	44.5135		3rd	43.7	44.915
	4th	59.62	60.0089		4th	59.8	60.8359

Dimensionless natural frequencies and critical buckling load of AFG Timoshenko beam

BC's		Fixed-Free			Hinged-Hinged	
n	Mode	Natural frequencies, $\overline{\omega}$	Buckling load (P_{cr})	Mode	Natural frequencies, $\overline{\omega}$	Buckling load (P_{cr})
0.2	1st	3.362	1.126	1st	7.509	3.286
	2nd	13.893		2nd	22.806	
	3rd	29.260		3rd	39.691	
	4th	43.925		4th	50.807	
0.3	1st	3.510	1.235	1st	7.585	3.518
	2nd	14.206		2nd	23.0653	
	3rd	29.6739		3rd	40.135	
	4th	44.469		4th	51.4253	
0.5	1st	3.705	1.409	1st	7.689	3.905
	2nd	14.629		2nd	23.430	
	3rd	30.288		3rd	40.766	
	4th	45.333		4th	52.318	
0.8	1st	3.854	1.599	1st	7.786	4.361
	2nd	14.966		2nd	23.763	
	3rd	30.828		3rd	41.356	
	4th	46.162		4th	53.207	
1.1	1st	3.914	1.735	1st	7.852	4.720
	2nd	15.141		2nd	23.957	
	3rd	31.172		3rd	41.717	
	4th	46.746		4th	53.803	
1.4	1st	3.929	1.834	1st	7.900	5.013
	2nd	15.240		2nd	24.077	
	3rd	31.424		3rd	41.952	
	4th	47.199		4th	54.231	
1.7	1st	3.922	1.909	1st	7.938	5.255
	2nd	15.300		2nd	24.153	
	3rd	31.624		3rd	42.112	
	4th	47.569		4th	54.552	
2.0	1st	3.904	1.967	1st	7.969	5.459
	2nd	15.339		2nd	24.204	
	3rd	31.791		3rd	42.222	
	4th	47.878		4th	54.8008	

As it is seen in Table 12, the power index parameter n has an increasing effect on both the natural frequencies and the critical buckling load.

Variation of the natural frequencies of a rotating axially functionally graded Timoshenko beam with respect to the dimensionless angular speed $\overline{\Omega}$ and the hub radius parameter σ is demonstrated in Figs. 9a–9b for $n = 1$. Since Zirconia's strength resistance for tension is very low, for the rotating beam model Ti-6Al-4V Alloy is used instead of ZrO_2 at the fixed end and pure Al is used at the free end. For Ti-6Al-4V, the modulus of elasticity $E_{Ti} = 110$ GPa, the material density $\rho_{Ti} = 4429$ kg/m^3.
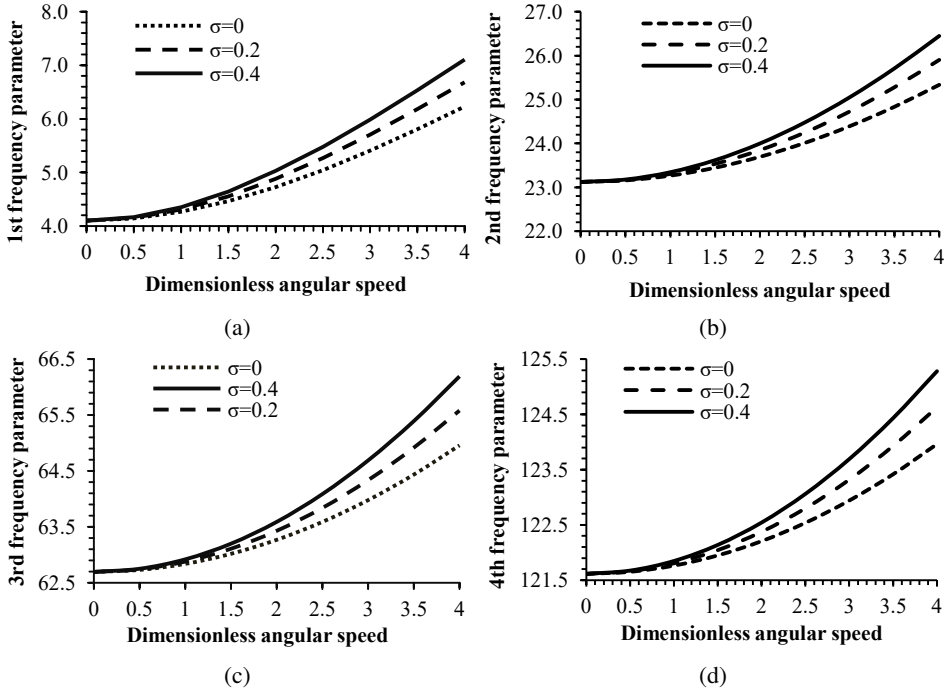
Fig. 9. Variations of various natural frequency parameters, $\overline{\omega}$, with hub radius and dimensionless angular speed: (a) 1st natural frequency parameter, $\overline{\omega}_1$; (b) 2st natural frequency parameter, $\overline{\omega}_2$; (c)3rd natural frequency parameter, $\overline{\omega}_3$; (d) 4th natural frequency parameter, $\overline{\omega}_4$

As it is seen in Figs. 9a–9d, the natural frequencies increase with the increasing dimensionless angular speed, $\overline{\Omega}$ and this rate of increase becomes larger with increasing hub radius parameter σ because, as interpreted by Eq. (4), the centrifugal force has a larger effect on the natural frequencies when the hub radius parameter is increased.

7. Conclusions

Finite element method is applied to carry out vibration and stability analyses of rotating/nonrotating, homogeneous/axially functionally graded Euler-Bernoulli and Timoshenko beams. Mass and stiffness matrices are evaluated using the kinetic

and potential energy expressions of the studied beam models. Numerical examples are solved and effects of several parameters on both the natural frequencies and the critical buckling load are inspected, and the results are tabulated in several figures and tables. It is considered that:

- The natural frequencies increase with the increasing dimensionless angular speed $\overline{\Omega}$ and this rate of increase becomes larger with increasing hub radius parameter σ.
- Beams with hinged-hinged boundary conditions have higher natural frequencies and buckling load values when compared to the beam with fixed-free end conditions.
- Beams with fixed-fixed boundary conditions have higher natural frequencies when compared to the beam with fixed-free end conditions.
- The power index parameter **n** has an increasing effect on both the natural frequencies and the critical buckling loads.

References

[1] C.T. Loy, K.Y. Lam, and J.N. Reddy. Vibration of functionally graded cylindrical shells. *International Journal of Mechanical Sciences*, 41(3):309–324, 1999. doi: 10.1016/S0020-7403(98)00054-X.

[2] B.V. Sankar. An elasticity solution for functionally graded beams. *Composites Science and Technology*, 61(5):689–696, 2001. doi: 10.1016/S0266-3538(01)00007-0.

[3] M. Aydogdu and V. Taskin. Free vibration analysis of functionally graded beams with simply supported edges. *Materials & Design*, 28(5):1651–1656, 2007. doi: 10.1016/j.matdes.2006.02.007.

[4] A. Chakraborty, S. Gopalakrishnan, and J.N. Reddy, A new beam finite element for the analysis of functionally graded materials. *International Journal of Mechanical Sciences*, 45(3):519–539, 2003. doi: 10.1016/S0020-7403(03)00058-4.

[5] A.J. Goupee and S.S. Vel. Optimization of natural frequencies of bidirectional functionally graded beams. *Structural and Multidisciplinary Optimization*, 32:473–484, 2006. doi: 10.1007/s00158-006-0022-1.

[6] H.J. Xiang and J. Yang. Free and forced vibration of a laminated FGM Timoshenko beam of variable thickness under heat conduction. *Composites Part B:Engineering*, 39(2):292–303, 2008. doi: 10.1016/j.compositesb.2007.01.005.

[7] M.T. Piovan and R. Sampaio. A study on the dynamics of rotating beams with functionally graded properties. *Journal of Sound and Vibration*, 327(1-2):134–143, 2009. doi: 10.1016/j.jsv.2009.06.015.

[8] M Şimşek and T. Kocatürk. Free and forced vibration of a functionally graded beam subjected to a concentrated moving harmonic load. *Composite Structures*, 90(4):465–473, 2009. doi: 10.1016/j.compstruct.2009.04.024.

[9] P. Malekzadeh, M.R. Golbahar Haghighi, and M.M. Atashi. Out-of-plane free vibration of functionally graded circular curved beams in thermal environment. *Composite Structures*, 92: 541–552, 2010. doi: 10.1016/j.compstruct.2009.08.040.

[10] Y. Huang and X.F. Li. A new approach for free vibration of axially functionally graded beams with non-uniform cross-section. *Journal of Sound and Vibration*, 329(11):2291–2303, 2010. doi: 10.1016/j.jsv.2009.12.029.

[11] A. Shahba, R. Attarnejad, M.T. Marvi, and S. Hajilar. Free vibration and stability analysis of axially functionally graded tapered Timoshenko beams with classical and non-classical boundary conditions. *Composites Part B: Engineering*, 42(4):801–808, 2011. doi: 10.1016/j.compositesb.2011.01.017.

[12] I. Elishakoff and Y. Miglis. Some intriguing results pertaining to functionally graded columns. *Journal of Applied Mechanics*, 80(4):1021–1029, 2013. doi: 10.1115/1.4007983.

[13] M. Soltani and B. Asgarian. New hybrid approach for free vibration and stability analyses of axially functionally graded Euler-Bernoulli beams with variable cross-section resting on uniform Winkler-Pasternak foundation. *Latin American Journal of Solids and Structures*. 16(3):e173, 2019. doi: 10.1590/1679-78254665.

[14] J.H. Kim and G.H. Paulino. Isoparametric graded finite elements for nonhomogeneous isotropic and orthotropic materials.*Journal of Applied Mechanics*, 69(4):502–514, 2002. doi: 10.1115/1.1467094.

[15] P. Zahedinejad, C. Zhang, H. Zhang, and S. Ju. A comprehensive review on vibration analysis of functionally graded beams. *International Journal of Structural Stability and Dynamics*, 20(4):2030002, 2020. doi: 10.1142/S0219455420300025.

[16] N. Zhang, T. Khan, H. Guo, S. Shi, W. Zhong, and W. Zhang. Functionally graded materials: An overview of stability, buckling, and free vibration analysis. *Advances in Material Science and Engineering*, 1354150, 2019. doi: 10.1155/2019/1354150.

[17] Ö. Özdemir. Application of the differential transform method to the free vibration analysis of functionally graded Timoshenko beams. *Journal of Theoretical and Applied Mechanics*. 54(4):1205–1217, 2016.

[18] B. Kılıç. *Vibration analysis of axially functionally graded rotor blades*. Msc.Thesis, Istanbul Technical University, İstanbul, Turkey, 2019.

[19] S. Rajasekaran. Differential transformation and differential quadrature methods for centrifugally stiffened axially functionally graded tapered beams. International Journal of Mechanical Sciences. 74. 15-31, 2013.

[20] A.D. Wright, C.E. Smith, R.W. Thresher, and J.L.C. Wang. Vibration modes of centrifugally stiffened beams. *Journal of Applied Mechanics*. 49(1):197–202, 1982. doi: 10.1115/1.3161966.